Influence of ground motion on the time evolution of beams in linear colliders

Andrey Sery* and Olivier Napoly
Commissariat à l'Energie Atomique, Departement de Science de Matériaux,
Département d'Astrophysique de Physique des Particles de Physique Nucléaire et de l'Instrumentation Associée
Centre d'Etudes Nucléaires de Saclay, F-91191 Gif-sur-Yvette Cedex, France
(Received 5 September 1995, revised manuscript received 19 December 1995)

This paper resumes a series of investigations devoted to the influence of ground motion on linear colliders in the TeV energy range. We attempt to model a variety of measured ground motion data and then to calculate the behavior of beams in the linear collider affected by this motion. An adequate description of ground motion is found in the form of a two-dimensional power spectrum $P(\omega,k)$ that carries information both about the time and space dependences of displacements. We then discuss the use of this spectrum to calculate the time evolution of beam position and beam size at the interaction point. A few approximations of this spectrum for typical seismic conditions are proposed for a wide range of ω and k based on the results of absolute and relative seismic measurements. Examples of calculations of the time evolution of the beam size and position in the final focus system of a linear collider are presented. Estimations of the influence of feedback are made.

PACS number(s): 41.75.Ht, 29.17.+w, 29.27.−a, 41.85.−p

I. INTRODUCTION

A. Linear colliders

In order to allow an effective search of new particles, e^+e^- linear colliders envisioned for the future [1] should provide a center of mass energy in the range of 300 GeV −1 TeV with a luminosity as high as 10^{33}–10^{34} cm^{-2} s^{-1}. Given the expression of the luminosity

$$\mathscr{L}=f_{\mathrm{rep}}N^2/(4\pi\sigma_x^*\sigma_y^*), \tag{1}$$

where f_{rep} is the repetition rate of collisions of the e^+ and e^- bunches, N is the number of particles per bunch and, σ_x^* and σ_y^* are the transverse rms sizes of the bunch at the collision point, the possible set of parameters of the existing projects [2] is as follows: repetition rate f_{rep} = 10–1000 Hz, number of particles $N=10^{10}$–10^{11}, horizontal size $\sigma_x^*=0.25$–2 μm, and vertical size $\sigma_y^*=3$–30 nm.

One of the most critical parameters is the extremely small vertical size of the beam at the interaction point and therefore the very small value required of the vertical emittance of the beam. Proper alignment of the focusing and accelerating elements of a linear collider is necessary to achieve high luminosity. The most obvious effect of misaligned focusing lenses is that the e^+ and e^- bunches can simply miss each other at the collision point. Even if the bunches collide, their emittance can already be degraded during acceleration in the linear accelerators or dispersion can appear in the focusing section before collision, due to misalignment. This degradation affects, in turn, the vertical spot size and the luminosity.

The tolerable misalignments are so small (less than 1 μm) that no conventional measurement technique can be used to maintain the required alignment. Moreover, a once aligned collider does not stay aligned forever because of ground motion. The only way to achieve required luminosity seen up to now is to have a rough prealignment with conventional technique and then to use the bunches themselves as sensors to detect the position of misaligned elements relative to the trajectory of the bunch. Therefore the alignment should be ''beam based'' and also it should be dynamical (i.e., the alignment should work continuously), to provide required stability of the alignment. A prototype of such a scheme has already been applied on the Stanford Linear Collider (SLC) [3].

The goal of this work is to derive a mathematically consistent model describing ground motion and to use it to predict the evolution of the beam properties with time over wide range of time intervals—from a few pulses to years—eventually taking the dynamical beam-based alignment into account.

B. Ground motion description

When the importance of ground motion for a linear collider was recognized, attempts were made to get the necessary information to describe this motion. A pioneering work was done at the Stanford Linear Accelerator Center (SLAC) [4] to understand the influence on a 50-GeV linear collider, for which the ground motion was already not negligible. For TeV linear colliders many studies have been made. Investigations of different ground motion characteristics were made at Protrino Branch of the Institute of Nuclear Physics [5] and since then similar studies have been made and are being continued by many other workers at Novosibirsk Institute of Nuclear Physics (INP) [6], Organisation Européenne pour la Recherche Nucléaire (CERN) [7], National Laboratory for High Energy Physics (KEK) [8], Deutsches Elektronen-Synchrotron (DESY) [9], Finland Research Institute for High Energy Physics (SEFT) [10], and Stanford Linear Accelerator Center (SLAC) [11], etc. One can mention also seismic studies performed for large circular colliders [12,13], because some results obtained there can be interesting for a linear collider as well.

Let us briefly describe what kinds of measurements have been performed and what kind of information has been obtained in these studies. All measurements of ground motion

*Permanent address: Branch of the Institute of Nuclear Physics, 142284 Protvino, Moscow Region, Russia.

can be grouped into two categories. The first one is the so-called absolute measurements. In this case usually an accelerometer with a pendulum inside is used. One measures acceleration of a single point of the ground surface versus time. If the spectral analysis is then applied, the spectrum of displacements can be obtained from the acceleration spectrum. This method is called absolute measurements because the measurements are made relative to an inertial frame. The second category consists of the relative measurements. In this case the relative positions of two separated points of the surface are measured. Some reference line (strained wire, laser beam, water level in gravity field, etc.) must be used in this case. The first method is sometime refined: simultaneous measurements with two distanced and synchronized sensors can give correlation information.

1. Absolute measurements

Let us consider data treatment methods used in measurements of absolute motion. Once a time-dependent signal $x(t)$ is measured, one can introduce its variance σ^2 as

$$\sigma^2=\langle x^2\rangle=\lim_{T\to\infty}\frac{1}{T}\int_{-T/2}^{T/2}x^2(t)dt. \tag{2}$$

Here and below we assume that the mean value of the signal is zero $\langle x\rangle=0$, namely,

$$\langle x\rangle=\lim_{T\to\infty}\frac{1}{T}\int_{-T/2}^{T/2}x(t)dt=0. \tag{3}$$

Performing the spectral analysis of the signal is useful because different vibration frequencies cause different effects on the linear collider and should be considered in different ways. One should note, however, that a seismic signal is a random process, so the power spectral density (power spectrum in brief) should be considered instead of the usual Fourier spectrum.

The power spectral density is defined as

$$p(f)=\lim_{T\to\infty}\frac{1}{T}\left|\int_{-T/2}^{T/2}x(t)e^{-i\omega t}dt\right|^2. \tag{4}$$

Here f is frequency $f=\omega/2\pi$. One of the main properties of the power spectrum is that its integral gives the variance

$$\sigma^2=\int_{-\infty}^{\infty}p(f)df. \tag{5}$$

In practice the measurement time T is limited and the power spectrum can only be estimated by averaging spectra obtained from several measurements. The number of averagings $n_{\rm av}$ fixes the precision of the estimation of this spectrum ($\Delta p/p\propto 1/\sqrt{n_{\rm av}}$); usually it is not better than a few percent. Also, the measurement technique with discrete sampling requires one to replace the integral by a discrete sum in the formulas. Data measured over time T at sampling frequency f_0 allow one to find a spectrum in the range from $1/T$ to $f_0/2$. The dimension of the power spectrum is m^2/Hz if $x(t)$ is the position; sometimes it is more convenient to use $\mu\mathrm{m}^2/\mathrm{Hz}$. This kind of spectrum is usually plotted in logarithmic scale because of large changes over the frequency range.

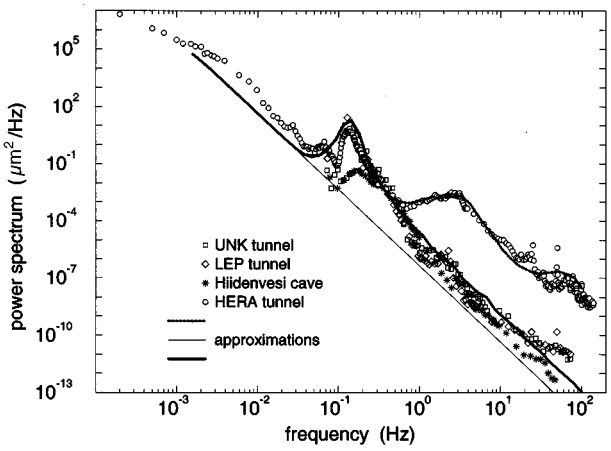

FIG. 1. Power spectra of absolute ground motion, measured in Protvino by Baklakov *et al.* [5]; CERN, Juravlev *et al.* [7]; DESY, Shiltsev *et al.* [9]; and Juravlev *et al.* in Finland [10].

Typical power spectra measured in different places are shown in Fig. 1. In this figure the measurements at Protvino (Russia) by Baklakov *et al.* in the 30-m underground tunnel of the UNK storage ring under construction [5]; at CERN by Juravlev *et al.*, 80 m underground, in the Large Electron-Positron (LEP) tunnel [7]; in a 100-m-deep (in horizontal direction) cave in a 30-m-high hill near Helsinki, Finland [10]; and by Shiltsev *et al.* in the underground Hadron Electron Ring Accelerator (HERA) tunnel at DESY [9] are shown. All spectra shown in Fig. 1, except the one by Shiltsev, were measured during a quiet time (i.e., night, when there is a minimum of cultural noises). The lines shown on the plot are approximations to be explained later. The frequency band of the data presented in this figure is limited by the working frequency range of the sensor, that is, the range where the signal to noise ratio of the electronics is sufficient. In order to cover a wider frequency band, different sensors with different self-frequencies of pendulum must be used.

The power spectra in Fig. 1 grow very fast with decreasing frequency. In quiet conditions they behave approximately as $p(f)\propto 1/f^4$ (compare with the straight line in this figure that corresponds to $1/f^4$) in a rather wide frequency band. Sources that contribute to the spectrum are different at different frequencies. At very low frequency $f<1$ Hz the main sources of ground motion are atmospheric activity, water motion in the oceans, temperature variations, etc. A well known example of the influence of water motion in the oceans is the peak in the band 0.1–0.2 Hz. This peak, is generated by the interaction of ocean waves with the coastline. Its amplitude depends slightly on the distance from the oceans: a significant reduction can be observed only in the central part of continents [6]. In general, vibrations in this low-frequency band $f<1$ Hz depend not only on the local conditions, but rather remote sources can give significant contribution to this slow motion.

From the other side, in the band $f>1$ Hz, the human produced noises usually dominate and the power spectrum depends very much on the local conditions (location of

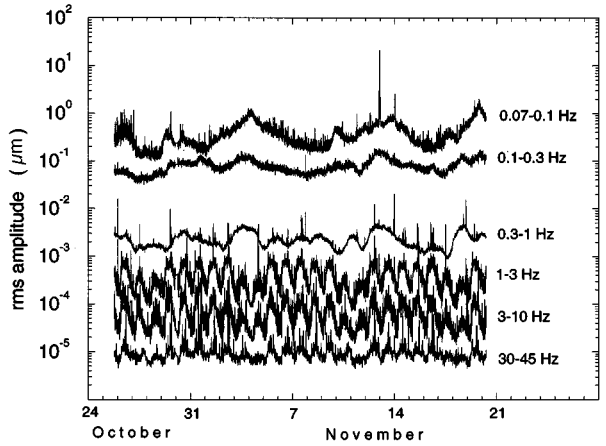

FIG. 2. The rms amplitude of different frequency bands versus time. The measurements were taken in Finland, October–November 1994 [10].

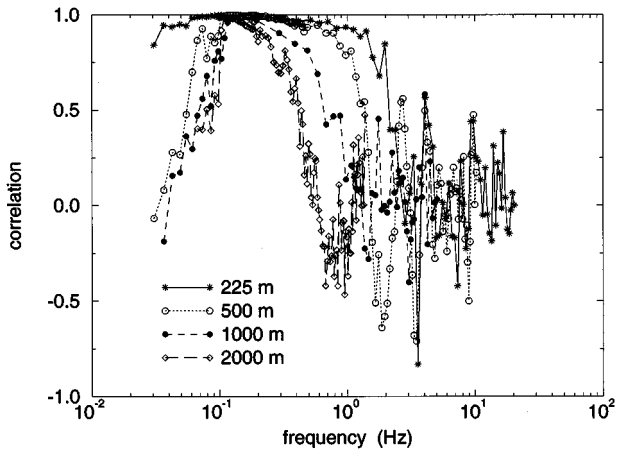

FIG. 3. Correlation spectra of ground motion measured at CERN in the LEP tunnel [7]. The distances between sensors were 225, 500, 1000, and 2000 m.

sources of noises, depth of tunnel etc.). For example, the spectrum measured by Shiltsev at DESY presents much larger amplitudes at $f>1$ Hz due to noises generated by different technical devices of the HERA collider and of the city.

The power spectrum allows one to identify contributions from different frequencies according to the formula

$$\sigma^2(f_0<f<f_1)=\int_{f_0}^{f_1}p(f)df. \tag{6}$$

This is illustrated by Fig. 2, where the contributions of different frequency bands to the rms amplitude are shown. This plot is the result of continuous measurements by Juravlev *et al.* in Finland in the Hiidenvesi cave [10]. In the high-frequency part the rms amplitude is one order of magnitude larger during the working hours than during the nighttime and holidays. The smooth variation of amplitudes in the low-frequency part is due mainly to weather variations above the ocean and sharp isolated peaks are earthquakes, usually remote.

One should note that since the power spectrum of a real signal is symmetrical, it is sufficient to consider only positive frequencies with the proper normalization. In all figures in this paper the measured spectra are defined so that the integral for only positive f in (5) is equal to the variance (2). However, in all formulas [except (6)] we will use spectra defined from $-\infty$ to $+\infty$ in such a way that (5), for example, is valid.

2. Correlation measurements

The absolute measurements, performed simultaneously by two sensors, allow one to find the mutual power spectrum of two signals x_1 and x_2:

$$p_{12}(f)=\lim_{T\to\infty}\frac{1}{T}\int_{-T/2}^{T/2}x_1(t)e^{-i\omega t}dt\int_{-T/2}^{T/2}x_2^*(t')e^{i\omega t'}dt'. \tag{7}$$

In contrast with $p(f)$ this spectrum is complex. For a real signal $x(t)$ one can write $p_{12}^*=p_{21}$, so that the imaginary part is given by

$$2i\ \mathrm{Im}(p_{12})=p_{12}-p_{21}. \tag{8}$$

One can note that if characteristics of ground motion do not depend on the location, then this imaginary part should be equal to zero. This condition is assumed to always be satisfied.

The normalized mutual power spectrum can also be used:

$$N_{12}(f)=\frac{p_{12}}{\sqrt{p_1p_2}}. \tag{9}$$

The real part of N_{12} is called ''correlation'' and its module is called ''coherence.'' According to the above-mentioned assumption, N_{12} will be real and $p_1=p_2$ and N_{12} will depend on the distance between points but not on their position.

Perfect correlation between the two points corresponds to $N_{12}(f)=1$, the absence of correlations to $N_{12}(f)=0$, and perfect anticorrelation (phase shift π) to $N_{12}(f)=-1$. Similar to the power spectrum, in practice the estimation of the correlation can be found by averaging several measurements. The relative precision in this case depends also on the correlation itself:

$$\frac{\Delta N_{12}}{N_{12}}\propto\sqrt{\frac{1-N_{12}}{n_{\mathrm{av}}}}. \tag{10}$$

In a simple case when there are only transverse waves that propagate along the line connecting two probes, the waves have phase velocity v, there is no dissipation, and the sources of the waves are remote enough, the correlation (9) will be equal to

$$N_{12}(f)=\cos(\omega L/v), \tag{11}$$

where L is the distance between the probes. If the distribution of the directions of propagation is uniform on the azi-

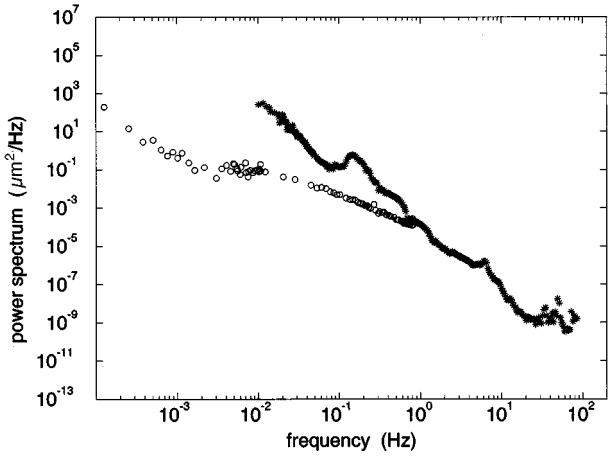

FIG. 4. Comparison of the spectrum of relative ground motion [at a distance of 5 m between probes (circles)] with the spectrum of absolute ground motion (stars), measured by Baklakov *et al.* in the laboratory building in Protvino [14].

muthal angle θ, then the correlation is equal to the average $\langle \cos[\omega L/v \cos(\theta)] \rangle_\theta$, which gives Bessel function

$$N_{12}(f) = J_0(\omega L/v). \tag{12}$$

An example of the correlation measured in the CERN LEP tunnel by Juravlev *et al.* [7] is shown in Fig. 3. Different curves correspond to different distances between sensors. One can see a good correlation in the low-frequency part $f > 0.1$ Hz of the spectrum. At high frequencies the correlation between separated probes disappears. These measurements have shown that the correlation at $f > 0.1$ Hz can be approximated by (11) with the parameter $v(f)$ close to the velocity of sound (about 3000 m/s at $f \approx 0.1$ Hz in that case).

At smaller frequency $f < 0.1$ Hz decreasing correlation has been observed [5,7,9], resulting in much smaller values of $v(f)$, which may hint at the presence of non-wave-like motion at these frequencies. However, since the signal to noise ratio of the probes used becomes poor also at these frequencies, further studies seem to be necessary, preferably using cross-checks by relative measurements.

3. Relative measurements

Measurements of relative motion give information about the quantity $x_1(t) - x_2(t)$. The power spectrum $\rho(\omega, L)$ associated with it is given by

$$\rho(\omega, L) = \lim_{T \to \infty} \frac{1}{T} \left| \int_{-T/2}^{T/2} [x_1(t) - x_2(t)] e^{-i\omega t} dt \right|^2 \tag{13}$$

in such a way that

$$\langle [x(t, s+L) - x(t,s)]^2 \rangle = \int_{-\infty}^{\infty} \rho(\omega, L) d\omega / (2\pi). \tag{14}$$

It depends explicitly on the distance L between points of measurements. Note that $\rho(\omega, L)$ and $p(\omega)$ have the same dimension (m^2/Hz).

An example of the spectrum of relative motion of two points separated by 5 m is shown in Fig. 4. The measurements were performed by Baklakov *et al.* in the laboratory building in Protvino using the strained wire technique with pickup sensors mounted on the tables [14]. On the same plot the results of the absolute measurements by Baklakov *et al.* at the same place are shown. The amplitudes in this spectrum are large compared with the quiet spectra of Fig. 1 because of noisy conditions in the laboratory. This example demonstrates the typical behavior of such spectra: the amplitudes of relative motion are much smaller than those of absolute motion at low frequencies (the spectrum of relative motion grows only as $1/f^2$). At some high frequency where correlations disappear they become similar.

Figure 4 shows results of relative measurements for relatively high frequencies. There is also a lot of data about relative measurements performed with the geodesic technique. The time scale of these data is usually days or years and distances are of the order of hundreds of meters. A typical example of such data is the measurements of the long time scale displacements of the SLC tunnel studied by Fischer and Morton [15].

It was found in [5] that data about slow relative motion measured in different sites of the world can be described by a simple expression

$$\langle \Delta X^2 \rangle = ATL, \tag{15}$$

where ΔX is the relative displacement after a time T of the two points separated by a distance L. A is a constant whose value was found to be $A \approx 10^{-4}$ μm^2 s^{-1} m^{-1} and the variation of this value for different places in the world is not much more than one order of magnitude [5,16]. In some special places with granite or limestone surroundings, the values $A \approx 10^{-6}$ μm^2 s^{-1} m^{-1} were found [17]. The formula (15) is known as the ''ATL law.''

One can see that the displacement in (15) is proportional to the square root of the time: this stresses the random, non-wave-like diffusional character of the slow relative motion. The square root dependence on the distance L can be understood by supposing that the number of steplike breaks that appear between two points is proportional to the distance between them. There are also more complex explanations of these dependences; for example, in [18], a fractal model of ground was developed to explain this behavior.

The ranges of T and L where the ATL law is valid are very wide. In [16] it was summarized that (15) is confirmed by measurements of ground motion in different accelerator tunnels in the range from minutes to tens of years and from a few meters to tens of kilometers.

Although the ATL law was found from the direct analysis of measurements of ground motion, its most interesting confirmations come from the observations of beam motion in large accelerators produced by displacements of the focusing elements. For example, the measurements of the closed orbit motion in the HERA circular collider have shown that the power spectrum of this motion corresponds to the ATL law in a wide frequency range, from $f \approx 1$ Hz (for larger frequencies cultural noises were significant) down to $f \approx 10^{-6}$ Hz (limited by the time of these observations) [19].

C. Using measured data

Let us discuss now how the available measured data of ground motion can be used for studying the stability of a linear collider. One can see that the power spectrum of absolute motion itself does not contain all the necessary information. Indeed, measurements show (see above) that this spectrum behaves approximately as $p(f)\propto 1/f^4$ in a rather wide frequency range. One can notice that this spectrum, if it behaves so at low frequencies too, gives an infinite value for the variance that is typical of a random signal. This is so also for the difference of the absolute displacements with finite time separation τ. The associated variance is given by the integral [20]

$$\langle [x(t+\tau)-x(t)]^2\rangle_t = \int_{-\infty}^{\infty} p(f)2[1-\cos(\omega\tau)]df, \qquad (16)$$

which is also infinite in this assumption [21]. Equation (16) shows that the low-frequency motion ($\omega \ll 1/\tau$) contributes to the integral with an attenuation factor $(\omega\tau)^2$, but it is still not enough to make the integral finite. The integral on the power spectrum over a certain frequency band, as in (6), also cannot be used easily without additional correlation information. However, for the stability of linear colliders one is only interested in relative displacements between two elements separated by a distance L and hence in the spectrum of relative motion $\rho(\omega,L)$.

Let us try to obtain this spectrum $\rho(\omega,L)$ from the spectrum of absolute motion. In principle, it can be done if simultaneous absolute measurements by two probes are performed. These spectra are connected as follows:

$$\rho(\omega,L)=p_1(\omega)+p_2(\omega)-p_{12}(\omega,L)-p_{21}(\omega,L), \quad (17)$$

where p_1, p_2 and p_{12}, p_{21} are the usual and mutual spectra, respectively. Assuming that the spectra of these two signals are the same $p_1=p_2=p(\omega)$, one can rewrite (17) using the definition of the correlation as

$$\rho(\omega,L)=p(\omega)2\{1-\mathrm{Re}[N_{12}(\omega,L)]\}. \qquad (18)$$

At first sight it seems that the spectrum of relative motion can be extracted from the spectrum of absolute motion using (18). But, in practice, it is possible only in a certain frequency range. At high frequencies the signal to noise ratio of the instrument becomes poor. At low frequencies this ratio can be good, but in this case the interesting uncorrelated part of motion usually has much smaller amplitudes than the correlated part. So, because of the intrinsic imperfection of absolute measurements, the correlation cannot be measured with the necessary precision and formula (18) cannot be used below and above of certain frequencies. Typically, (18) can be used only for $0.1<f<100$ Hz.

The spectrum of relative motion can be obtained, of course, directly from relative measurements. The problem here is that the measurements can be performed only in some limited region of parameters (frequency or distance). For example, measurements by a water level system give information only about slow motion. The strained wire technique can measure fast vibrations also, but the distance between measured points is limited for this method as for the previous one. Optical methods have problems of accuracy over long distances. So there is no ideal instrument for measuring the characteristics of ground motion. Therefore both absolute and relative measurements should be used in complement to each other in order to cover a wider range of parameters.

There is one essential drawback of using the spectrum of relative motion $\rho(\omega,L)$: it does not separate contributions from different spatial wavelengths to the relative motion of two points. These contributions may have very different impact on the linear collider stability, especially for wavelengths close to harmonics of betatron wavelengths. This is the main reason why a new mathematical tool describing ground motion needs to be built that incorporates results from both absolute and relative measurements and at the same time is adequate to calculate beam stability in linear colliders.

II. GENERALIZED DESCRIPTION OF GROUND MOTION

A. Two-dimensional power spectrum of ground motion

As already mentioned, TeV linear colliders are very sensitive to ground motion. But, of course, if ground motion would displace the linear collider as a whole rigid body, it would not influence its operation. Rather smooth changes of the shape of the collider do not have much of an effect either. For example, vibrations with long spatial periods similar to waves from the ocean have a very small influence on the linear collider in spite of their large amplitudes. On the other hand, vibrations with spatial periods of a few tens of meters can have a great effect, even though their amplitudes are much smaller. Thus it is necessary to have information about both time and spatial characteristics of ground motion. An adequate description of ground motion is through the two-dimensional power spectrum proposed in [10].

Let us denote by s the longitudinal position of an element along a linear collider and $x(t,s)$ the transverse position of this element, which depends also on the time t. The displacement $x(t,s)$ is an absolute one, i.e., it is measured relative to an infinitely remote object. We consider only transverse displacements of elements because they are known to have the most significant influence on a linear collider.

One can introduce a two-dimensional power spectrum of this displacement $x(t,s)$ as

$$P(\omega,k)=\lim_{T\to\infty}\lim_{L\to\infty}\frac{1}{T}\frac{1}{L}\left|\int_{-T/2}^{T/2}\int_{-L/2}^{L/2}x(t,s)e^{-i\omega t}e^{-iks}dtds\right|^2, \qquad (19)$$

where $k=2\pi/\lambda$ and λ is the spatial period of displacements. We will see later that this spectrum contains all the necessary information for a linear collider.

The two-dimensional spectrum (19) contains information about both relative and absolute motion. For example, it is related to the one-dimensional spectrum by the formula

$$p(\omega)=\int_{-\infty}^{\infty}P(\omega,k)dk/2\pi. \qquad (20)$$

The variance of the displacement $x(t,s)$ is then given by

$$\sigma^2=\int_{-\infty}^{\infty}\int_{-\infty}^{\infty}P(\omega,k)d\omega dk/(2\pi)^2. \qquad (21)$$

It should, of course, be infinite, as it is for the usual spectrum, since the integral extends down to $\omega=0$.

Other spectral characteristics can be determined from this two-dimensional power spectrum. For example, the real part of the normalized mutual power spectrum (9) for two points separated by the distance L is equal to

$$\mathrm{Re}\,[N_{12}(\omega)]=\frac{\int_0^\infty P(\omega,k)\cos(kL)dk}{\int_0^\infty P(\omega,k)dk}. \tag{22}$$

For a linear collider we have to know the behavior of the relative displacements of two elements of the collider. Let us assume for simplicity that at the beginning ($t=0$) the collider is perfectly aligned and let us introduce the misalignment after the time T: $X(T,s)=x(t=T,s)-x(t=0,s)$. Then the variance of the relative misalignment over a distance L and after a time T is given by

$$\begin{aligned}\sigma^2(T,L)&=\langle[X(T,s+L)-X(T,s)]^2\rangle\\&=\int_{-\infty}^{\infty}\int_{-\infty}^{\infty}P(\omega,k)2[1-\cos(\omega T)]\\&\quad\times 2[1-\cos(kL)]d\omega dk/(2\pi)^2.\end{aligned} \tag{23}$$

This is a main formula to evaluate linear collider stability with the help of the two-dimensional power spectrum.

B. Approximation of the two-dimensional power spectrum

Unlike the absolute $p(\omega)$ and relative $\rho(\omega,L)$ power spectra, the two-dimensional power spectrum $P(\omega,k)$ is not directly measured in an experiment. But if one knows $p(\omega)$ and $\rho(\omega,L)$ for a wide enough range of parameters, one can determine the two-dimensional power spectrum through the identities

$$\rho(\omega,L)=\int_{-\infty}^{\infty}P(\omega,k)2[1-\cos(kL)]dk/2\pi \tag{24}$$

and, for the back transformation,

$$P(\omega,k)=\int_0^\infty\cos(kL)[\rho(\omega,L=\infty)-\rho(\omega,L)]dL. \tag{25}$$

In (25) $\rho(\omega,L=\infty)$ is equal to $2p(\omega)$ [see (18)] because correlations vanish at $L=\infty$.

The approximation for $\rho(\omega,L)$ will be made on the assumption that the low-frequency part of motion is described by the ATL law, while the high-frequency part is produced mainly by waves but with a small, poorly correlated high-frequency tail of the ATL law.

Let us consider the twodimensional spectrum that corresponds to the motion described by the ATL law (15), which can be written as

$$P(\omega,k)=\frac{A}{\omega^2k^2}, \tag{26}$$

which can be easily shown by direct substitution of (26) into (23) and comparison with (15). The relative spectrum $\rho(\omega,L)$ for the ATL law is then given by

$$\rho(\omega,L)=\frac{AL}{\omega^2}. \tag{27}$$

We are going to use this formula as an approximation of $\rho(\omega,L)$ in the region of parameters where it does not contradict measured data or where it is known to work. This formula can be used as an approximation of $\rho(\omega,L)$ only in the region of small frequencies because it behaves like $1/\omega^2$, while the spectrum of absolute motion in a quiet place behaves like $1/\omega^4$. Thus, for some high frequencies (27) will contradict to the condition $\rho(\omega,L)\leqslant 2p(\omega)$, which follows from (18). Therefore the spectrum of the ATL law (27) should be corrected at high frequencies.

In order to correct (27) let us consider correlation measurements at high frequencies. At $f>0.1$ Hz the absolute motion was found to be well correlated because of its wavelike character. However, the limited precision of sensors leaves room for the assumption that some fraction of motion is uncorrelated. To find the upper limit of the effects one can make the conservative assumption that all motion below the resolution of the probes is uncorrelated. In this assumption the uncorrelated part in measurements [7] corresponds approximately to the thin line in Fig. 1 given by $p(\omega)=B/2\omega^4$ with $B=10^{-3}\ \mu\mathrm{m}^2/\mathrm{s}^3$. Intending to find an upper limit of the effect, one may suppose that ATL law is valid as long as the condition $B/\omega^4>AL/\omega^2$ is satisfied. This results in the following approximation for the $\rho(\omega,L)$ of the ''corrected ATL law'':

$$\rho(\omega,L)=\begin{cases}AL/\omega^2 & \text{if } 0<\omega<\omega_0\\ B/\omega^4 & \text{if } \omega_0<\omega<\infty,\end{cases} \tag{28}$$

where $\omega_0=(B/AL)^{1/2}$. From Eq. (28) one then obtains the following approximation for the power spectrum $P(\omega,k)$ of the corrected ATL law:

$$P(\omega,k)=\frac{A}{\omega^2k^2}[1-\cos(L_0k)], \tag{29}$$

with $L_0=B/(A\omega^2)$.

The exact result for the variance of the relative misalignment corresponding to (29) is given, from Eq. (23), by

$$\begin{aligned}\langle\Delta X^2\rangle&=ATL+ATL\,\frac{2}{\pi}\left(\mathrm{Si}(2x_0)-\frac{1-\cos(2x_0)}{2x_0}\right)\\&\quad+\frac{BT^3}{6\pi}\left(2\,\mathrm{Si}\,(2x_0)+\frac{\cos(2x_0)}{x_0}\right.\\&\quad\left.+\frac{\sin(x_0)[\sin(x_0)+x_0\cos(x_0)]}{x_0^3}\right),\end{aligned} \tag{30}$$

where $x_0=T/2\sqrt{B/(LA)}$ and $\mathrm{Si}(x)$ is defined as

$$\mathrm{Si}(x)=-\int_x^\infty\frac{\sin(t)}{t}dt. \tag{31}$$

One can show from this formula that the chosen form of the $P(\omega,k)$ spectrum gives a square root dependence of the relative misalignment versus time for large T (corresponding to the ATL law):

$$\langle \Delta X^2 \rangle = ATL, \quad T \gg T_0, \tag{32}$$

while for small T the relative misalignment is just proportional to the time T:

$$\langle \Delta X^2 \rangle = AT^2 L/T_0, \quad T \ll T_0, \tag{33}$$

where $T_0 = \pi/2\sqrt{AL/B}$. One can note that this linear dependence of the rms displacement at small time is the general property of the spectrum that drops fast enough with increasing frequency [22]. In fact, with reasonable accuracy one can use the simple formula

$$\langle \Delta X^2 \rangle \approx ATL \frac{T}{T+T_0} \tag{34}$$

as an approximation of (30).

The contribution from elastic waves may be added to the spectrum $P(\omega,k)$ as

$$P(\omega,k) = \frac{A}{\omega^2 k^2}[1-\cos(L_0 k)] + D(\omega)U(\omega,k). \tag{35}$$

The function $U(\omega,k)$ describes the wave number distribution of the waves with frequency ω. The expression

$$U(\omega,k) = \begin{cases} \dfrac{2}{\sqrt{k_{\max}^2 - k^2}} & \text{if } |k| \leqslant k_{\max} \\ 0 & \text{if } |k| > k_{\max} \end{cases} \tag{36}$$

corresponds to transverse waves propagating at the surface of the ground with a uniform distribution over the azimuthal angle, with $k_{\max}(\omega) = \omega/v_i$ and v_i the velocity of wave propagation. The cases $k=0$ and $k=k_{\max}$ correspond to the waves propagating perpendicular and along the linear collider correspondingly.

Since the integral over $dk/(2\pi)$ of $U(\omega,k)$ equals one, the function $D(\omega)$ describes the contribution of these waves to the absolute spectrum $p(\omega)$. Writing $D(\omega)$ as

$$D(\omega) = \frac{a_i}{1+[d_i(\omega-\omega_i)/\omega_i]^4} \tag{37}$$

allows one to take into account the peak of the waves from the oceans and also, because of the $1/\omega^4$ dependence, to add some wave contribution at high frequencies. In order to model more complex behavior of the spectrum, for example, the in presence of cultural noises, a few terms $D(\omega)U(\omega,k)$ may be added to $P(\omega,k)$; in that case i would be the number of the peak. Assuming that the parameters of (35) do not depend significantly on ω or k, the four models corresponding to different conditions or assumptions will be considered in the following subsection.

C. Approximations for different conditions

We will consider four different models based on (35). The first three models have the same power spectrum $p(\omega)$ corresponding to quiet conditions, such as in the LEP or UNK tunnels studied by Juravlev *et al.* or Baklakov *et al.* but with a different k dependence of $P(\omega,k)$. The fourth model will correspond to conditions of the HERA DESY tunnel measured by Shiltsev *et al.* which is known to have large contributions from cultural noises.

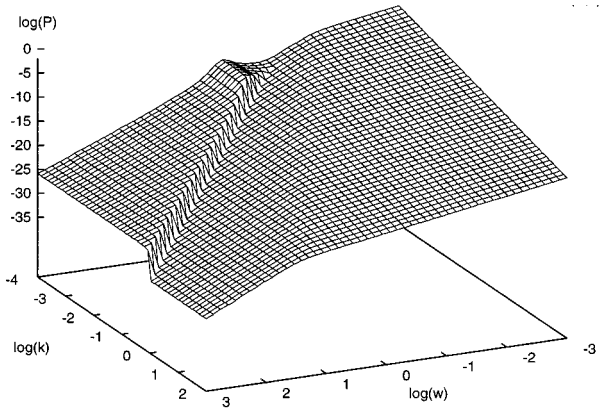

FIG. 5. Three-dimensional logarithmic (with decimal base $\log_{10}$) plot of the power spectrum $P(\omega,k)$ corresponding to model 1 of ground motion.

The parameters of the first model (model 1) are $A = 10^{-4}\ \mu\text{m}^2\,\text{s}^{-1}\text{m}^{-1}$ and $B = 10^{-3}\ \mu\text{m}^2/\text{s}^3$. The single peak described by $\omega_1 = 2\pi \times 0.14$ Hz for the frequency of the peak, $a_1 = 10\ \mu\text{m}^2/\text{Hz}$ for its amplitude, $d_1 = 5$ for its width, and $v_1 = 1000$ m/s for the velocity. The resulting approximation of the two-dimensional spectrum $P(\omega,k)$ for model 1 is shown in Fig. 5 [with the $1-\cos(\xi)$ term in (35) replaced by $1/(1+2/\xi^2)$ to smooth the plot]. The absolute power spectrum calculated from this analytic form of $P(\omega,k)$ is plotted in Fig. 1 as a solid thick line: one can see that it is in good agreement with the LEP and UNK power spectra (Juraviev *et al.* and Baklakov *et al.*, respectively). The calculated correlation function $N_{12}(\omega,L)$ plotted in Fig. 6 behaves similarly to the measured one: it exhibits a decrease of correlation at high frequencies according to (12) and also vanishes in the band $f = 0.01$–0.1 Hz because of a large uncorrelated part of motions assumed for this model.

Model 1 should be considered as giving an upper limit of the effects of ground motion in quiet conditions since it assumes a rather large part of uncorrelated motion in the high-

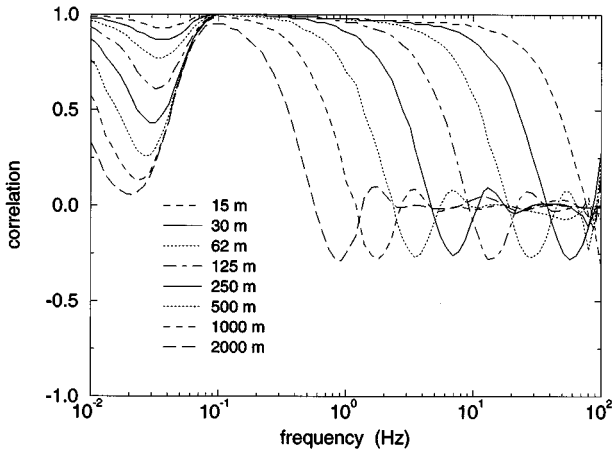

FIG. 6. Correlation spectra $N_{12}(\omega,L)$ calculated with the analytic model 1 of $P(\omega,k)$ for different distances between sensors.

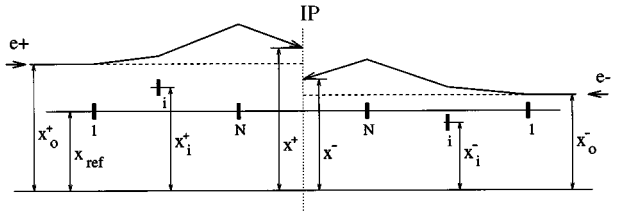

FIG. 7. Layout of the e^+ and e^- parts of a linear collider near the interaction region.

frequency band. Indeed, recent measurements by Adolphsen, Mazaheri, and Slaton at SLAC [23] have shown that the uncorrelated part is at least two orders of magnitude smaller [24] for $0.03<f<3$ Hz than it is assumed in model 1. More realistic assumption about the high-frequency part of motion results in model 2, which has the same parameters as model 1, but has $B=10^{-6}\ \mu\mathrm{m}^2/\mathrm{s}^3$.

Model 2, on the other hand, has a rather large value of the constant A, which can be considered as a pessimistic assumption if the site of the next linear collider tunnel is chosen properly or if an appropriate solid foundation (at least under the central part of the collider) is made. From this point of view one needs to consider also model 3, which is the same as model 2 but has $A=10^{-6}\ \mu\mathrm{m}^2\ \mathrm{s}^{-1}\ \mathrm{m}^{-1}$. This model should be considered as corresponding to a good tunnel built in an appropriate place where the influence of cultural noises is negligible.

One can also build an approximation (model 4) that corresponds to seismic conditions with large contributions from cultural noises (as in the HERA tunnel [9]). The parameters are $A=10^{-5}\ \mu\mathrm{m}^2\ \mathrm{s}^{-1}\ \mathrm{m}^{-1}$ (this value corresponds to the recent measurements in HERA [19]), $B=10^{-3}\ \mu\mathrm{m}^2/\mathrm{s}^3$, and three additional peaks: $\omega_1=2\pi\times 0.14$ Hz, $a_1=10\ \mu\mathrm{m}^2/\mathrm{Hz}$, $d_1=5$, and $v_1=1000$ m/s for the first peak; $\omega_2=2\pi\times 2.5$ Hz, $a_2=10^{-3}\mu\mathrm{m}^2/\mathrm{Hz}$, $d_2=1.5$, and $v_2=400$ m/s for the second; and $\omega_3=2\pi\times 50$ Hz, $a_3=10^{-7}\mu\mathrm{m}^2/\mathrm{Hz}$, $d_3=1.5$, and $v_3=400$ m/s for the third. The thick dashed line in Fig. 1 shows the spectrum of absolute motion, calculated from $P(\omega,k)$, corresponding to these parameters. The parameters a_i and d_i have been chosen to fit the absolute spectrum, while the parameters v_i have been derived [25] from correlation measurements at the HERA tunnel [26] and measurements of the closed orbit motion in HERA [19].

The four models listed above cover a wide enough range of conditions or assumptions. The presented approximation has, of course, some uncertainties, especially in the transition from wave motion to diffusive motion, which could be improved [27] if the relevant measurement data were available. Nevertheless, we believe that the models presented should be useful to investigate the beam stability in a given collider design.

III. CALCULATION OF BEAM BEHAVIOR USING THE TWO-DIMENSIONAL POWER SPECTRUM

In this section we want to show how the two-dimensional power spectrum $P(\omega,k)$ can be used to describe the beam stability in a linear collider. We will restrict ourselves to the effects of displacements at the leading linear order on the relative beam offset and at the leading quadratic order on the beam spot size at the interaction point (IP).

A. Beam offset at the IP

We consider two sections of the linear collider are symmetrical relative to the IP (see Fig. 7). We assume that both channels have been perfectly aligned at the time $t=0$ on some reference coordinate [28] x_{ref}. Let x_i^+ be the transverse position of the focusing element i on the e^+ side and x_i^- on the e^- side measured at some later time T relative to some reference line as shown in Fig. 7. The elements are enumerated from the entrance of each channel, the first element having number 1 and the last before the IP number N. We assume that the positions of the beams at injection x_0^+ and x_0^- are related to the position of some element, say, a beam position monitor, at the entrance of the considered section [29]. With these assumptions, the time evolution of all the coordinates $(x_i^\pm)_{i=0,N}$ can be described by the two-dimensional (2D) power spectrum like in Eq. (23)

$$\langle[x_i^\pm(T)-x_j^\pm(T)]^2\rangle=\int_{-\infty}^{\infty}\int_{-\infty}^{\infty}P(\omega,k)2[1-\cos(\omega T)]\times 2\{1-\cos[k(s_i^\pm-s_j^\pm)]\}d\omega dk/(2\pi)^2, \tag{38}$$

where $s_i^\pm$ is the longitudinal position of the ith element in the e^+ and e^- beam lines.

The most harmful effect of focusing element displacements for the luminosity is the transverse offset (x^+-x^-) of the opposite beams at the IP. Let a_i be the first derivative of the beam transverse displacement at the IP with respect to the displacement of the element i. At first order, the e^+ and e^- beam offsets at the IP are given by

$$x^\pm-x_{\mathrm{ref}}=R_{11}(x_0^\pm-x_{\mathrm{ref}})+\sum_{i=1}^{N}a_i(x_i^\pm-x_{\mathrm{ref}}), \tag{39}$$

where R is the transfer matrix of the section. We have assumed that the coefficients a_i are the same for the e^- and the e^+ parts. They can be easily calculated using optical functions of the channel. For example, for a short quadrupole, $a_i=k_i r_{12}$, where k_i is the integrated strength of the quadrupole and r_{12} is the element of transfer matrix from this element to the IP (for horizontal displacements, for the vertical one should take r_{34}). By considering a rigid displacement of the whole beam line, with $x_0=x_i=x$, it is easy to show that they satisfy the identity

$$\sum_{i=1}^{N}a_i=1-R_{11}. \tag{40}$$

Since only the relative displacement of the beams at the IP influences the luminosity, one can write, for this relative offset,

$$x^+-x^-=\sum_{i=0}^{N}a_i(x_i^+-x_i^-), \tag{41}$$

with the notation

$$a_0 = R_{11}. \tag{42}$$

The mean value $\langle x^+ - x^- \rangle$ is equal to zero. The mean square value is given by

$$\langle (x^+ - x^-)^2 \rangle = \sum_{i=0}^{N} \sum_{j=0}^{N} a_i a_j \langle (x_i^+ - x_i^-)(x_j^+ - x_j^-) \rangle. \tag{43}$$

To relate the above expression to the variance calculated from the 2D spectrum by Eq. (38), one uses the identity

$$(x_1 - x_2)(x_3 - x_4) = \tfrac{1}{2}[(x_1 - x_4)^2 + (x_2 - x_3)^2 - (x_1 - x_3)^2 - (x_2 - x_4)^2]. \tag{44}$$

Assuming that the spectrum $P(\omega,k)$ is homogeneous in such a way that $\langle (x_i^+ - x_j^+)^2 \rangle = \langle (x_i^- - x_j^-)^2 \rangle$ and $\langle (x_i^+ - x_j^-)^2 \rangle = \langle (x_i^- - x_j^+)^2 \rangle$, one gets, for the mean square of the relative beam offset,

$$\langle (x^+ - x^-)^2 \rangle = \sum_{i=0}^{N} \sum_{j=0}^{N} a_i a_j [\langle (x_i^+ - x_j^-)^2 \rangle - \langle (x_i^+ - x_j^+)^2 \rangle]. \tag{45}$$

Combining this expression with Eq. (23) allows one to calculate, from a given model of the 2D power spectrum $P(\omega,k)$, the time evolution of the rms relative offset after the time $t=0$ when it is zero.

For a pure ATL motion it is simply given by

$$\langle (x^+ - x^-)^2 \rangle = AT \sum_{i=0}^{N} \sum_{j=0}^{N} a_i a_j (|s_i^+ - s_j^-| - |s_i^+ - s_j^+|). \tag{46}$$

In general, Eq. (45) can be expressed as

$$\langle (x^+ - x^-)^2 \rangle = \int_{-\infty}^{\infty} \int_{-\infty}^{\infty} P(\omega,k) 2[1 - \cos(\omega T)] G(k) \frac{d\omega}{2\pi} \frac{dk}{2\pi}, \tag{47}$$

with the spectral function $G(k)$ given by

$$G(k) = \sum_{i=0}^{N} \sum_{j=0}^{N} 2 a_i a_j \{\cos[k(s_i^+ - s_j^+)] - \cos[k(s_i^+ - s_j^-)]\}. \tag{48}$$

By taking the origin of the longitudinal coordinate $s=0$ at the IP, one has $s_i^+ = -s_i^-$ and the above expression simplifies to

$$G(k) = 4 \left(\sum_{i=0}^{N} a_i \sin(k s_i^+) \right)^2. \tag{49}$$

The positive function $G(k)$ describes the spectral response to harmonic excitations of the spatial period of $2\pi/k$, of the focusing section considered, in terms of relative displacement of beams at the IP. For large k it fluctuates around N (if all $|a_i| \approx 1$). For harmonics with long wavelengths it is proportional to k^2, except when $R_{12}=0$, which is the most interesting case of beam lines with a phase advance equal to a multiple of π. Indeed one can easily show by tilting the whole beam line by a constant angle x_0' that the coefficients a_i verify to a good approximation, namely, for thin lenses, the identity

$$\sum_{i=0}^{N} a_i s_i + R_{12} = s_{\mathrm{IP}}. \tag{50}$$

Since we took $s_{\mathrm{IP}}=0$ in Eq. (49), one gets, for small k,

$$G(k) \simeq 4[kR_{12} + O(k^3)]^2 \tag{51}$$

showing that the spectral function $G(k)$ behaves as k^6 for $k \to 0$ if $R_{12}=0$.

Once $G(k)$ has been calculated for a given focusing structure, Eq. (47) is useful for comparing the behavior of beams through this structure in different seismic conditions. It also allows one to calculate the effect of different parts of the spatial wave-number spectrum.

B. Beam spot size at the IP

Transverse displacements of focusing elements can generate other effects at the IP. For example, for the final focus system of a linear collider the next most important effect is the spot size growth at the IP induced by dispersion, longitudinal shift of the beam waists, and xy coupling generated by offset beams in quadrupoles and sextupoles. At first order in the normalized transfer matrix error at the IP

$$\delta Q = \delta R R^{-1}. \tag{52}$$

The vertical spot size growth is given by

$$\frac{\delta \sigma_y^*}{\sigma_y^*} = \frac{1}{2} \left[\left(\frac{\delta Q_{34}}{\beta_y^*} \right)^2 + \left(\frac{\delta Q_{31} \sigma_x^*}{\sigma_y^*} \right)^2 + \left(\frac{\delta Q_{32} \sigma_x^*}{\sigma_y^* \beta_x^*} \right)^2 + \left(\frac{\delta Q_{36} \sigma_\delta}{\sigma_y^*} \right)^2 \right]. \tag{53}$$

The first term corresponds to the β_y waist shift generated by quadrupole and sextupole horizontal displacements. The second and third terms correspond to xy and $x'y$ couplings and the fourth term to vertical dispersion generated by quadrupole and sextupole vertical displacements [30].

The spot size growth induced by these effects can be calculated as for the offset in Eq. (45) but with different coefficients. For instance, the vertical dispersion δQ_{36} can be written as

$$\eta_y^* = \delta Q_{36} = T_{336}(y_0 - y_{\mathrm{ref}}) + \sum_{i=1}^{N} b_i (y_i - y_{\mathrm{ref}}). \tag{54}$$

Again a constant translation of the whole beam line leads to the identity

$$\sum_{i=1}^{N} b_i = -T_{336} \tag{55}$$

in such a way that the dispersion error is given by

$$\delta Q_{36} = \sum_{i=1}^{N} b_i (y_i - y_0). \tag{56}$$

As for the offset rms, the dispersion rms error is then related to the 2D power spectrum through the equality

$$\langle (\delta Q_{36})^2 \rangle = \frac{1}{2} \sum_{i=1}^{N} \sum_{j=1}^{N} b_i b_j [\langle (y_i - y_0)^2 \rangle + \langle (y_j - y_0)^2 \rangle - \langle (y_i - y_j)^2 \rangle] \tag{57}$$

This expression can also be used to defined a spectral function $G_\eta(k)$ associated with the dispersion:

$$G_\eta(k) = \sum_{i=1}^{N} \sum_{j=1}^{N} b_i b_j \{1 - 2\cos[k(s_i - s_0)] + \cos[k(s_i - s_j)]\}. \tag{58}$$

By applying the same treatment to the other error terms in Eq. (53) and by summing them with the dispersion term, the time evolution of the vertical spot size of one beam can be calculated from the 2D power spectrum $P(\omega,k)$. Since the horizontal displacements are responsible for the degradation of the spot size induced by the waist shift δQ_{34} term, we will assume, in the next section, that the horizontal and the vertical ground motion are described by the same power spectrum.

IV. APPLICATION TO FINAL FOCUS SYSTEMS

The final focus system (FFS) of a linear collider is the special optical system placed immediately before the IP. It provides the required big demagnifications of the transverse beam dimensions down to the desired beam sizes at collision.

The FFS's optics is based on the SLC final focus system [31,32]. Big demagnifications result in strong focusing of the beam, which in turn leads to large chromatic aberrations. These aberrations are compensated in chromatic correction sections using bending magnets and sextupoles. Usually a final focus system has a first telescope, two dispersive sections for correction of the horizontal and vertical chromaticities, and a final telescope. The tightest tolerances to transverse magnet displacements are found in the FFS (last quadupoles and sextupoles). It is therefore natural to illustrate the use of the above formalism to describe the influence of ground motion on such systems.

An example of a FFS optics with magnet layout and betatron functions for TESLA [33] is shown in Fig. 8. The relevant beam parameters at the IP of the main existing linear collider projects are shown in Table I [2]. The final beam energy is 250 TeV. $\beta^*_{x,y}$ are the beta functions, $\sigma^*_{x,y}$ is the rms transverse beam size at the IP, σ_z is the rms bunch length, σ_δ is the rms relative energy spread within one bunch or one bunch train, and here $f_{\rm rep}$ is the repetition frequency of the bunch trains. Usually the repetition rate of collisions within the same train in the multibunch case is too high for the trajectory of a single bunch to be corrected separately. For TESLA, however, this repetition rate (shown in parentheses) may be small enough to allow some fast bunch to bunch correction scheme. One can see from Table I that the vertical beam sizes at the IP are much smaller than the horizontal ones. We therefore concentrate on the time stability of the vertical offset and spot size, which are expected to set the most severe tolerances on displacement.

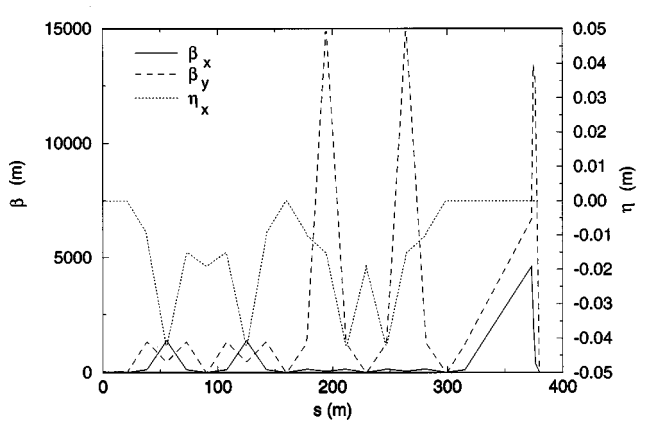

FIG. 8. Dispersion η_x and beta functions β_x and β_y of the TESLA FFS [33].

A. Beam stability in different conditions

The linear response of the FFS optics to ground motion is mainly characterized by the dimensionless coefficients a_i and b_i defined above, namely, the ratio of the vertical beam displacement and dispersion at the IP to the vertical displacement of each magnet indexed by i. These coefficients are plotted in Fig. 9 for each magnet of the TESLA FFS. One can see from these plots that the main contribution to the beam displacement at the IP comes from the two last quadrupoles, while the main sources of dispersion errors are the first two lenses of the last telescope.

Calculated from these coefficients with Eqs. (49) and (58), the spatial spectral functions $G(k)$ and $G_\eta(k)$ associated with the vertical relative offset and dispersion are plotted in Fig. 10. For small k, $G_\eta(k)$ behaves as k^4 and $G(k)$ exhibits the k^6 behavior predicted in Eq. (51) over a small range only.

The time evolution of the rms relative vertical beam offset, the vertical beam dispersion, and the spot size at the IP of some FFSs are shown in Figs. 11–13 assuming a perfectly aligned system at $t=0$. They are calculated as explained in the Sec. III from the 2D power spectrum $P(\omega,k)$ corresponding to model 1. The offset and dispersion curves of different colliders behave almost identically because of the similarity of the FFS designs. The spot size growth at the IP results mainly from the dispersion (also from waist shift and $x'y$ coupling for colliders with small energy spread), therefore the size growth $\delta\sigma/\sigma$ is smaller (at a given time) for the projects with large σ^*_y and small σ_δ.

The effects of different models can be seen in Figs. 14 and 15, where the vertical beam offset and dispersion at the IP of TESLA FFSs are shown. The difference between models 1 and 3 is about one order of magnitude (two orders of magnitude in luminosity $\delta\mathscr{L}/\mathscr{L}$), which shows an uncertainty gate of our assumptions about ground motion in quiet conditions. One can see that for models 1 and 2 the short

TABLE I. Beam parameters at the IP of final focus systems of TESLA (TeV Energy Superconducting Linear Accelerator), SBLC (S-Band Linear Collider), JLC (Japan Linear Collider), NLC (Next Linear Collider), VLEPP (Colliding Linear Electron Positron Beams), and CLIC (Compact Linear Collider).

Parameter	TESLA	SBLC	JLC	NLC	VLEPP	CLIC
$\beta^*_{x,y}$(mm)	25,0.7	22,0.8	10,0.1	10,0.1	100,0.2	10,0.18
$\sigma^*_{x,y}$(nm)	845,19	678,30	260,3	320,3.2	2000,6	250,7.5
σ_z(mm)	0.7	0.5	0.09	0.1	0.75	0.2
f_{rep}(Hz)	5 (1.4×10^6)	50	150	180	300	3200
$10^3\sigma_\delta$	1	5	2	2	5	2

time behavior of the beam offset is defined by the high-frequency tail of the *ATL* law and the wave contribution is not seen yet, while for model 3 at small times these waves give the main effect. Model 4 gives much larger values at small times due to cultural noises. The long time offset or dispersion behavior is defined completely by the diffusive motion.

These comparisons show also that the impact of the cultural noise is very important for the short time correction of the offset jitter and is less important for the long time correction of the dispersion. For TESLA, for example, the tolerance on the vertical dispersion from 2% luminosity loss is around 4 μm: it is therefore set by the part of the spectrum governed by the *ATL* law. On the contrary, the tolerance on

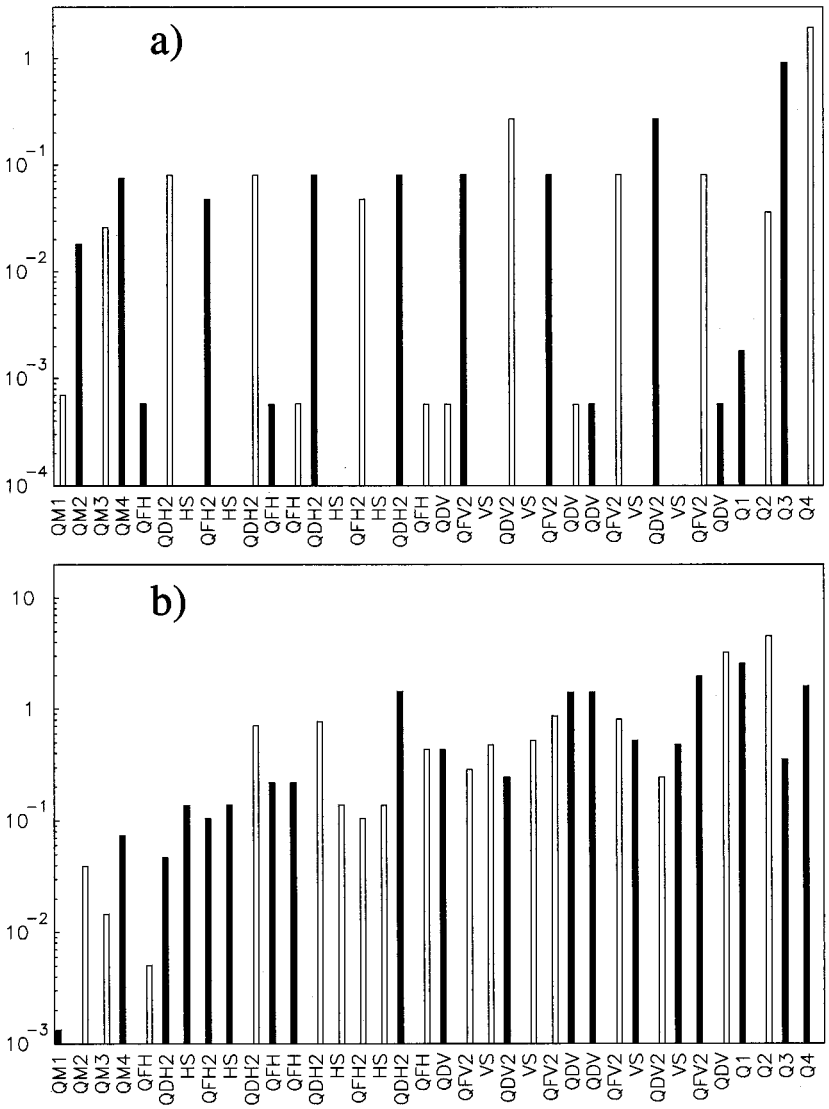

FIG. 9. Coefficients (a) a_i and (b) b_i, the ratios of the vertical beam displacement and dispersion at the IP to the displacement of each magnet, versus the magnet name for TESLA FFS. White bars correspond to positive values, black bars to negative ones.

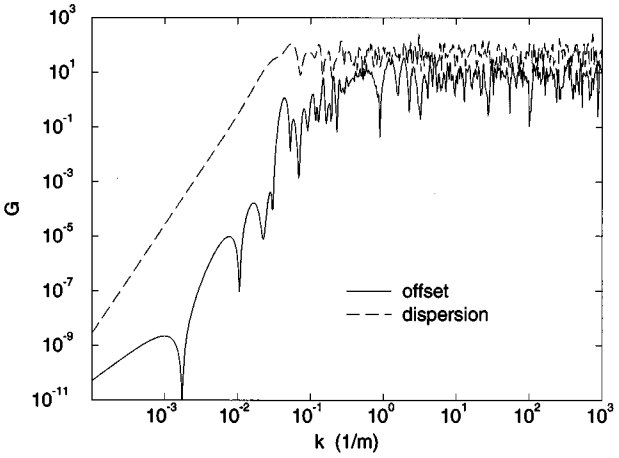

FIG. 10. Spectral response functions of the offset (G) and of dispersion (G_η) for the TESLA FFS.

the offset is around 5 nm and corresponds to the offset predicted after only 1 ms, which is roughly the length of one bunch train. This means that a continuous offset correction inside the TESLA bunch train would become required for a higher level of local noise.

The contribution of different wavelengths to the relative offset can be clearly seen in the integral

$$\int_0^k \frac{dk'}{2\pi} \int_0^\infty P(\omega,k')G(k')2[1-\cos(\omega T)]\frac{d\omega}{2\pi}, \qquad (59)$$

taken up to a given wave number k and normalized by its total value, i.e., by the rms offset according to Eq. (47). The regions of wave numbers where it increases rapidly are therefore the most dangerous ones. This integral is plotted in Fig. 16 for a TESLA FFS at time $T=0.03$ s. One can see that the range of critical wavelengths is from 100 m to a few meters, comparable to the lattice periods and β functions. One can see also that for models 1–3 some part of the contribution comes from the nonphysical range $\lambda<1$ m (typical value of the magnets length); this part is small, however, and can be neglected.

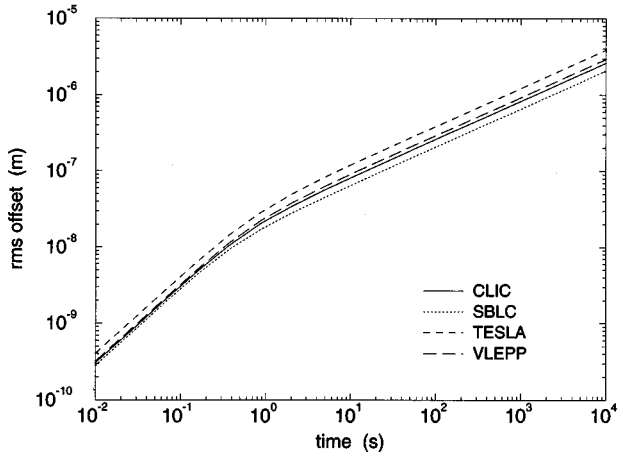

FIG. 11. Relative vertical rms offset of the beams at the IP versus time for the FFS of different linear colliders for model 1 of ground motion.

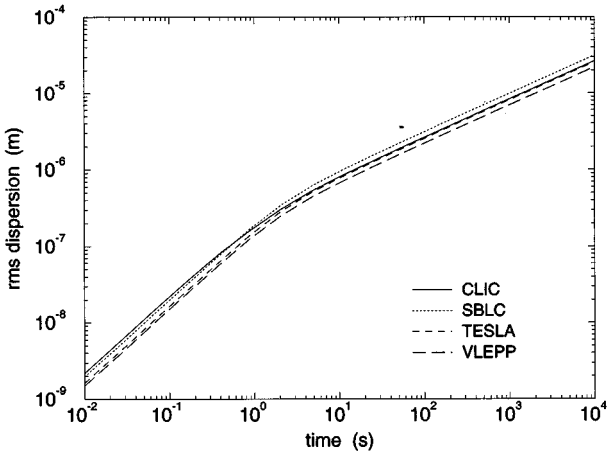

FIG. 12. Vertical rms dispersion of the beams at the IP versus time for the FFS of different linear colliders for model 1 of ground motion.

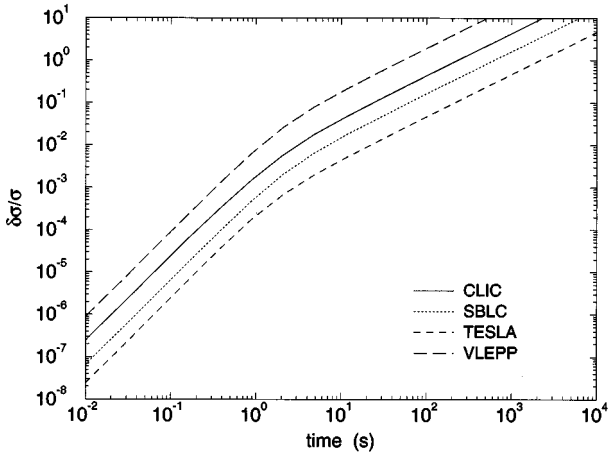

FIG. 13. Spot size growth at the IP versus time for the FFS of different linear colliders for model 1 of ground motion.

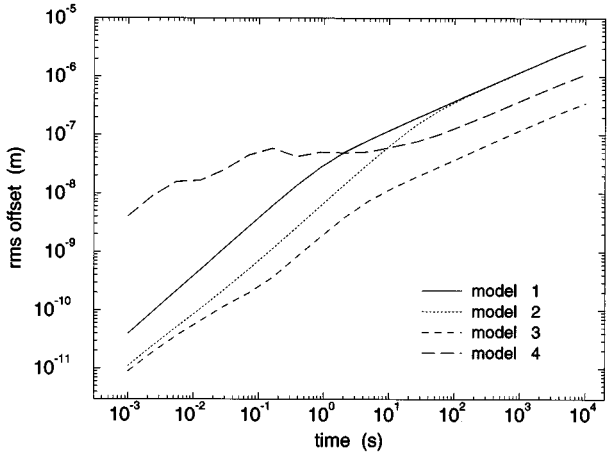

FIG. 14. Vertical relative rms offset of the beams at the IP for the TESLA FFS for different models of the power spectrum $P(\omega,k)$.

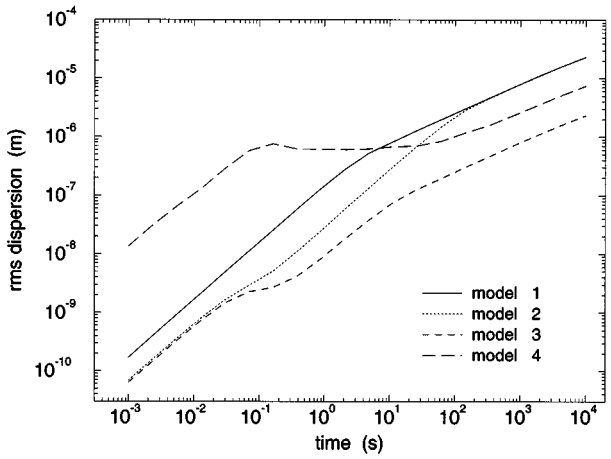

FIG. 15. Vertical rms dispersion at the IP of the TESLA FFS for different models of the power spectrum $P(\omega,k)$.

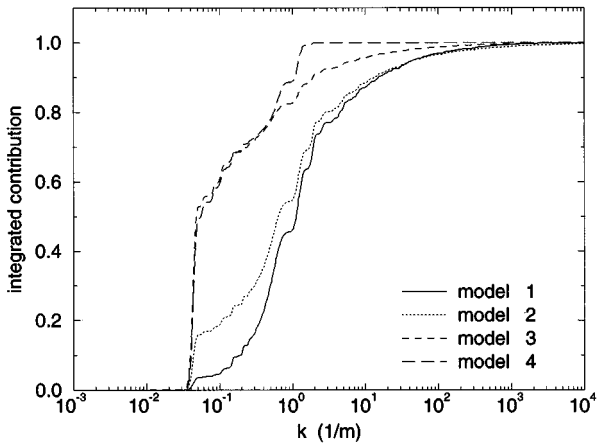

FIG. 16. Normalized integrated contribution of spatial harmonics from $k'=0$ up to $k'=k$ to the beam offset at the IP for the TESLA FFS at $T=0.03$ s for different models of the power spectrum.

From the relative offset and spot size variations one can derive the time corresponding to a loss of luminosity of 2% induced by either of these effects [34]. Then from the repetition rate given in Table I, one gets the corresponding number of pulses, reported in Table II for the models 1–3.

One can see from this table that the number of pulses corresponding to 2% luminosity loss due to beam offset caused by ground motion is small (except for CLIC, for which the situation is more relaxed due to a high repetition rate). It means that some fast feedback correction is necessary to keep the beam's head on at the interaction point. For TESLA a fast correction within each train seems to be desirable: the number of bunches colliding before 2% luminosity is lost then greatly exceeds the total number of bunches in one train (given in brackets).

If the offset of the beams at the IP is eliminated by a correction scheme, the luminosity degradation is due the growth of the beam spot size. The number of pulses before 2% luminosity loss is then of the order of 1000 for model 1 and much more for models 2 and 3. Some slow orbit correction scheme is thus also required to eliminate this effect.

A comparison of the models presented has shown that the uncertainty of the assumptions put in the base of the models and, to a greater extent, the uncertainty of local conditions (cultural noises, quality of the tunnel, etc.) warn us to be careful in applying the results to a specific project or to a particular site. Detailed measurements of ground motion at the specific site seem to be necessary to obtain correct quantitative predictions of beam behavior in particular conditions. We believe, nevertheless, that the present paper can serve as a framework for this task.

B. Effect of feedback

It has been shown that feedback corrections are necessary both for beam offset and for beam size stabilization. A consistent consideration of feedback correction schemes in the framework of the formalism presented requires further studies; however, some simple estimations of the capability of such corrections can be made easily.

A feedback correction scheme, for example, such as that applied on the SLC [3], can be characterized by the function F, which shows its performance. For example, it can be defined as the ratio $F(f)=p_{\rm on}(f)/p_{\rm off}(f)$, where $p_{\rm on}(f)$ and $p_{\rm off}(f)$ are the power spectra (of beam motion, for example) if the feedback is on and off correspondingly.

Let us consider feedback that corrects beam relative offset at the IP using the previous measurement. One can easily see that for small frequency f the performance of such feedback will be good: $F(f)=(f/f_c)^2$ for $f\ll f_c$, while at high frequencies the feedback gives no effect: $F(f)=1$ for $f\gg f_c$. In the ideal case $f_c=f_{\rm rep}/(2\pi)$. One can take, for simplicity, $F(f)=(f/f_c)^2$ for $f<f_c$ and $F(f)=1$ for $f>f_c$.

The effect of this feedback can be estimated in the following way. The equilibrium (i.e., at $T\to\infty$) value of the

TABLE II. Number of pulses corresponding to 2% luminosity loss due to relative vertical offset (N_{δ_y}) or vertical spot size growth ($N_{\sigma_y^*}$) at the IP of different projects for models 1–3 of ground motion in quiet conditions.

Parameter	Model	TESLA	SBLC	JLC	NLC	VLEPP	CLIC
$N_{\delta y}$	1	1 ($\gg$1000)	15	4	5	15	220
$N_{\delta y}$	2	4 ($\gg$1000)	75	22	27	77	1200
$N_{\delta y}$	3	15 ($\gg$1000)	370	60	75	260	4200
$N_{\sigma_y^*}$	1	210	650	370	450	540	17000
$N_{\sigma_y^*}$	2	350	1700	1800	2100	2700	66000
$N_{\sigma_y^*}$	3	21000	65000	18000	22000	30000	1.7×10^6

TABLE III. Estimations of equilibrium values of the rms vertical beam offset ($\delta y/\sigma_y^*$) caused by ground motion in quiet (models 1–3) and in noisy (model 4) conditions, in the presence of an ideal feedback with $f_c = f_{\rm rep}/30$.

Parameter	Model	TESLA	SBLC	JLC	NLC	VLEPP	CLIC
$\delta y/\sigma_y^*$	1	1.9 ($\ll 1$)	0.18	0.5	0.47	0.15	0.013
$\delta y/\sigma_y^*$	2	0.5 ($\ll 1$)	0.03	0.1	0.09	0.03	0.003
$\delta y/\sigma_y^*$	3	0.14 ($\ll 1$)	0.01	0.04	0.04	0.015	0.002
$\delta y/\sigma_y^*$	4	2.9 ($\ll 1$)	2.0	10	9	3.5	1.2

offset in the presence of the feedback is

$$\langle (x^+ - x^-)^2 \rangle_\infty \to \int_{-\infty}^{\infty} \int_{-\infty}^{\infty} P(\omega,k) 2F(\omega) G(k) \frac{d\omega}{2\pi} \frac{dk}{2\pi}. \tag{60}$$

Here we assumed that $F(\omega)$ does not depend on k and feedback adds no errors to beam motion (due to errors of beam position measurements, for example); otherwise a term corresponding to the feedback-produced noises should be added to (60). Comparing Eqs. (60) and (47), one can see that for the chosen $F(\omega)$ the following approximation can be written:

$$\langle (x^+ - x^-)^2 \rangle_\infty \approx \langle (x^+ - x^-)^2 \rangle \text{ at } T = \sqrt{2}/(2\pi f_c). \tag{61}$$

Using this expression and making a conservative assumption that $f_c = f_{\rm rep}/30$ (which corresponds to the value achieved at SLAC [3]; better values should be possible, however), one can find the equilibrium value of the offset for different colliders for different models of the power spectrum. The results are shown in Table III.

Table III shows that in quiet conditions the feedback with $f_c = f_{\rm rep}/30$ allows one to keep luminosity with precision much better than 2% for models 2 and 3 of ground motion. For the most pessimistic model 1 the value $\delta\mathscr{L}/\mathscr{L}$ is about 6% (since $\delta\mathscr{L}/\mathscr{L} \approx -[\delta y/(2\sigma_y^*)]^2$). One can qualitatively conclude that in a quiet place the luminosity losses due to beam offset caused by ground motion can be eliminated by a feedback correction. Again, the correct quantitative prediction for particular conditions requires detailed studies of a specific feedback scheme, including an analysis of feedback produced errors. On the other hand, in noisy conditions (model 4) significant luminosity losses can be avoided only if a faster orbit correction (such as bunch to bunch) or additional stabilization of magnet positions is used.

V. CONCLUSION

The influence of ground motion is expected to be very important for future TeV linear colliders. It will require precise alignment techniques probably combined with damping of the magnet vibrations. To describe this influence quantitatively in terms of beam properties and luminosity at the IP, we propose to use the power spectrum $P(\omega,k)$, previously introduced by one of the present authors. This two-dimensional power spectrum describes both the time and spatial properties of ground motion. It also encompasses the power spectra associated with the absolute and the relative displacements such as the ATL law describing slow diffusive motion. Various expressions of this spectrum can be made to model the information about absolute and relative measurements of ground motion. We have derived four such models to account for typical low or high cultural noise conditions.

We then described the formalism, which allows one to express the time evolution of typical beam properties, such as beam offset, dispersion, or spot size, for a beam line submitted to transverse vibrations corresponding to a given power spectrum $P(\omega,k)$ of ground motion. This formalism has been applied to analyze the sensitivity of various final focus systems for linear collider designs to ground vibrations over short and long time ranges, using and comparing different approximations of the power spectra. Finally, in the framework of the formalism considered, a capability of feedback to keep luminosity has been estimated.

ACKNOWLEDGMENTS

The authors would like to thank Stéphane Fartoukh for help in the calculations; John Irwin for extremely helpful discussions, many suggestions, and a thorough reading of the manuscript; and Vladimir Balakin, Reinhard Brinkmann, Alban Mosnier, Vladimir Shiltsev, Shigeru Takeda, and Nick Walker for useful discussions.

[1] KEK Report KEK Proceedings 95-5, 1995 (unpublished).
[2] SLAC Report No. SLAC-R-95-471, 1995 (unpublished).
[3] L. Hendrickson *et al.*, SLAC Report No. SLAC-PUB-6621, 1994 (unpublished).
[4] G. E. Fischer, SLAC Report No. SLAC-PUB-3392 Rev., 1985 (unpublished).
[5] B. A. Baklakov, P. K. Lebedev, V. V. Parkhomchuk, A. A. Sery, A. I. Sleptsov, and V. D. Shiltsev, INP Report 91-15, 1991 (unpublished).
[6] V. A. Lebedev, P. K. Lebedev, V. V. Parkhomchuk, and V. D. Shiltsev, INP Report 92-39, 1992 (unpublished).
[7] V. M. Juravlev, A. A. Sery, A. I. Sleptsov, W. Coosemans, G. Ramseier, and I. Wilson, CERN Report No. SL/93-53, 1993 (unpublished).
[8] S. Takeda, A. Akiyama, K. Kudo, H. Nakanishi, and N. Yamamoto, KEK Report 93-61, 1993 (unpublished).
[9] V. Shiltsev, B. Baklakov, P. Lebedev, C. Montag, J. Rossbach, DESY HERA Report No. 95-06, 1995 (unpublished).
[10] V. M. Juravlev, P. A. Lunev, A. A. Sery, A. I. Sleptsov, K. Honkavaara, R. Orava, and E. Pietarinen, SEFT Report HU-

SEFT R 1995-01, 1995 (unpublished).
[11] C. Adolphsen and M. Ross (unpublished).
[12] J. Rossbach, DESY Report No. 89-023, 1989 (unpublished).
[13] V. Parkhomchuk, V. Shiltsev, and H. J. Weaver SSCL Report 323, 1993 (unpublished).
[14] B. A. Baklakov, P. K. Lebedev, V. V. Parkhomchuk, A. A. Sery, A. I. Sleptsov, and V. D. Shiltsev, Zh. Tekh. Fiz. **63**, 122 (1993) [Tech. Phys. **38**, 894 (1993)].
[15] G. E. Fischer and P. Morton, SSCL Report 55, 1986 (unpublished).
[16] V. Parkhomchuk, V. Shiltsev, and G. Stupakov, Part. Accel. **46**, 241 (1994).
[17] Shigeru Takeda (private communication).
[18] V. Parkhomchuk and V. Shiltsev, INP Report 92-31, 1992 (unpublished).
[19] R. Brinkmann and J. Rossbach, Nucl. Instrum. Methods Phys. Res. Sect. A **350**, 8 (1994).
[20] This formula can be obtained using the parity of $p(f)$ and the theorem that the autocorrelation $\langle x(t+\tau)x(t)\rangle_t$ and the power spectrum $p(f)$ are connected via Fourier transformation.
[21] This assumption fails at very small frequencies, resulting in a finite answer for the integral (16); this does not affect the results of the paper.
[22] S. Fartoukh, O. Napoly, and A. Sery, Centre d'Etudes Nucléaires de Saclay Report No. 95-05, 1995 (unpublished).
[23] C. Adolphsen, G. Mazaheri, and T. Slaton (unpublished).
[24] This was pointed out to us by John Irwin.
[25] A. Sery and O. Napoly (unpublished).
[26] V. Shiltsev, B. Baklakov, P. Lebedev, J. Rossbach, and C. Montag, DESY HERA Report No. 95-06, 1995 (unpublished).
[27] Allowing the constants A and B in (28) to depend on ω and L could help to make this improvement.
[28] This reference coordinate x_{ref} may vary along the line; this does not affect the main results of this paragraph.
[29] The case where the beam is injected with an angle is not considered in this paper.
[30] The linear contribution from the vertical demagnification error δQ_{33} is usually negligible.
[31] K. L. Brown, J. J. Murray, and T. Fieguth, Stanford Linear Accelerator Center Report No. 4219, 1986 (unpublished).
[32] O. Napoly, T. Taylor, and B. Zotter, CERN Report No. CH-1211, 1989 (unpublished).
[33] O. Napoly, E. Klein, and J. Rifflet, Centre d'Etudes Nucléaires de Saclay Report No. 94-10, 1994 (unpublished).
[34] The tolerances to offset do not take the beam-beam attraction into account.